ATMOSPHERIC SCIENCE

On the fate of oxygenated organic molecules in atmospheric aerosol particles

V. Pospisilova[1], F. D. Lopez-Hilfiker[1,2], D. M. Bell[1], I. El Haddad[1], C. Mohr[3], W. Huang[4], L. Heikkinen[5], M. Xiao[1], J. Dommen[1], A. S. H. Prevot[1], U. Baltensperger[1], J. G. Slowik[1]*

Highly oxygenated organic molecules (HOMs) are formed from the oxidation of biogenic and anthropogenic gases and affect Earth's climate and air quality by their key role in particle formation and growth. While the formation of these molecules in the gas phase has been extensively studied, the complexity of organic aerosol (OA) and lack of suitable measurement techniques have hindered the investigation of their fate post-condensation, although further reactions have been proposed. We report here novel real-time measurements of these species in the particle phase, achieved using our recently developed extractive electrospray ionization time-of-flight mass spectrometer (EESI-TOF). Our results reveal that condensed-phase reactions rapidly alter OA composition and the contribution of HOMs to the particle mass. In consequence, the atmospheric fate of HOMs cannot be described solely in terms of volatility, but particle-phase reactions must be considered to describe HOM effects on the overall particle life cycle and global carbon budget.

INTRODUCTION

Atmospheric aerosols influence Earth's climate by scattering or absorbing solar radiation and by changing the physical properties of clouds (*1*). The oxidation of organic gases such as α-pinene, one of the globally dominating biogenic vapors, leads to the formation of oxygenated volatile organic compounds (OVOCs) with a broad volatility range (*2*). Highly oxygenated organic molecules (HOMs) are a subset of OVOCs (*3*), characterized by substantially reduced saturation vapor pressures, which therefore play an important role in new particle formation and the growth of newly formed particles to cloud condensation nuclei (CCN) size (*4*). From a thermodynamic perspective, HOM condensation would constitute an irreversible transfer of mass to the particle phase and represent a sink of gaseous organics if the chemistry governing HOM production and depletion were to occur predominantly in the gas phase. While the gas phase has been extensively studied in laboratory and field settings by various chemical ionization methods (*5*, *6*), real-time observations of particle-phase HOMs at atmospheric concentrations remain limited by low time resolution, high detection limits, suboptimal ionization schemes, and/or thermal decomposition (*7*–*9*), leading to reduced chemical resolution and/or substantial uncertainty in the particle composition. As a result, while further reactions in the particle phase have been proposed, their nature remains unclear (*2*, *10*). A number of studies have attempted to investigate particle-phase HOMs by using aerosol collection followed by offline chemical analyses. This approach provides detailed structural information and, in some cases, molecular identification but, due to low time resolution and/or reaction during sample transfer and storage (*11*), leaves the role of rapid physico-chemical processes highly uncertain. In particular, the effects and time scales of condensed-phase reactions affecting the overall particle life cycle and global carbon budget are poorly constrained (*12*).

Here, we present real-time measurements of oxygenated particulate organics (including HOMs) that are not subject to thermal desorption, ionization-induced fragmentation, competitive ionization pathways, or separated sampling/analysis stages. This is achieved using a novel extractive electrospray ionization time-of-flight mass spectrometer (EESI-TOF) (*13*), which couples soft ionization with high time resolution to provide quasi-molecular composition (i.e., molecular formula) of continuously sampled aerosol. No currently existing technique can combine true molecular identification with real-time particle-phase analysis; our work thus represents a substantial advance in the chemical resolution available to real-time systems, providing previously inaccessible compositional and kinetic data that both complements and contrasts with state-of-the-art offline analyses. Here, we investigate secondary organic aerosol (SOA) formed from the ozonolysis of a monoterpene (α-pinene). Monoterpenes are among the most important SOA precursors in pristine regions of the world and are important even in anthropogenically influenced environments such as the southeastern United States and Central Europe (*8*, *14*). Our measurements reveal the particle phase to be a dynamic environment in which the chemical composition continuously evolves because of particle-phase decomposition of high–molecular weight HOMs. This implies that the atmospheric fate of HOMs cannot be described simply in terms of their volatility, but is also influenced by post-condensation reactions, affecting the contribution of HOMs to particulate mass, SOA composition, and volatility.

RESULTS

To discriminate between gas-phase production, condensation, and particle-phase reaction of HOMs from α-pinene ozonolysis, three fast oxidation batch-mode experiments were conducted in the 27-m³ Teflon chamber at the Paul Scherrer Institute. About 30 ppbv (parts per billion by volume) of α-pinene was injected into a dark chamber kept at room temperature, 40 to 50% relative humidity (RH), and prefilled with excess ozone (~400 ppbv; table S1; see experiment 1), giving an α-pinene:O₃ ratio consistent with conditions in the Finnish boreal forest (*15*–*17*).

[1]Laboratory of Atmospheric Chemistry, Paul Scherrer Institute, 5232 Villigen, Switzerland. [2]Tofwerk AG, 3600 Thun, Switzerland. [3]Department of Environmental Science, Stockholm University, Stockholm 11418, Sweden. [4]Institute of Meteorology and Climate Research, Karlsruhe Institute of Technology, 76344 Eggenstein-Leopoldshafen, Germany. [5]Institute for Atmospheric and Earth System Research, Faculty of Science, University of Helsinki, Helsinki 00014, Finland.
*Corresponding author. Email: jay.slowik@psi.ch

These conditions enabled fast SOA formation and minimized the loss of oxidized vapors to the wall. The reaction mixture was kept undisturbed for the next 12 hours with dilution of 30 liters min^{-1} to maintain the volume of the chamber. The particle-phase composition was measured by the EESI-TOF (with 1-s time resolution) and a Filter Inlet for Gases and AEROsols (FIGAERO) iodide chemical ionization mass spectrometer (CIMS) with ~50-min time resolution (18). A scanning mobility particle sizer (SMPS) was used to monitor the particle number size distribution and to calculate the total aerosol volume. Organic gases (α-pinene and its oxidation products) were monitored continuously by a proton transfer reaction time-of-flight mass spectrometer (PTR-TOF-MS) and a nitrate chemical ionization time-of-flight mass spectrometer (CIMS), and intermittently by an iodide CIMS. All signals from the EESI-TOF are reported in terms of the mass flux of ions to the detector of the mass spectrometer (in attograms per second). All ions are detected as adducts with Na^+, which, for simplicity, is removed from both the spectra and text (I^- and NO_3^- are likewise removed for the respective CIMS techniques). All particle-phase data presented here are corrected for particle wall loss based on the decay of the particle number concentration. A detailed description of the wall loss correction, chamber, and experiment setup and a brief description of all instruments can be found in Materials and Methods.

Figure 1A shows the EESI-TOF mass spectrum for experiment 1 (table S1), in which α-pinene–derived SOA (~23 μg m^{-3}) was generated. The mass spectrum is an average of 30 s taken at the point of maximum aerosol mass. Both monomers (C_5–C_{10}) and dimers (C_{15}–C_{20}) are evident. The monomer region is dominated by C_{10} and C_9 species, which make up 51% of the total signal. This spectrum is similar to the ambient mass spectrum shown in Fig. 1B, measured by the EESI-TOF during May 2017 field measurements in the boreal forest, conducted at the Station for Measuring Ecosystem-Atmosphere Relations (SMEAR II) in Hyytiälä, Finland (fig. S1), where the OA is typically dominated by monoterpene oxidation products. We note that based on the investigations of the wind trajectories above the canopy (fig. S2), the air mass can be influenced by the sawmill emissions, likely leading to terpene-dominated SOA (15, 17). The ambient OA mass concentration was about 14 μg m^{-3}, slightly lower than the chamber experiments, but similar patterns with molecular formulas $C_{5-10}H_{10-18}O_{3-10}$ in the monomer region and $C_{15-20}H_{24-34}O_{5-11}$ in the dimer region are observed for both chamber and ambient measurements. The overall spectral similarity is shown by a Pearson's R^2 value of 0.67 and a cosine similarity of 0.70; both these values are significantly higher than those obtained when comparing these spectra with ambient or laboratory spectra that are not terpene-related or correspond to mixed terpene/anthropogenic sources (see fig. S3). The main differences are the higher fraction of particle-phase oligomers in the chamber (~15% in Hyytiälä versus ~30% in chamber) and the presence of nitrogen-containing species in the ambient spectrum. The increased oligomer fraction in the chamber is consistent with recent findings showing that the particle-phase dimer fraction increases with the precursor concentration (19), as well as with the absence of NO_x in the chamber experiments, which suppresses gas-phase dimerization via the $RO_2\cdot + RO_2\cdot$ pathway in favor of organonitrate, peroxynitrate, or alkoxy radical formation (20), which are, in turn, consistent with the observation of nitrogen-containing species $C_{8-10}H_{11-17}O_{5-9}N$ at Hyytiälä. These organonitrates can alternatively be produced from the oxidation of monoterpenes by $NO_3\cdot$ radicals, as these events were observed during early morning
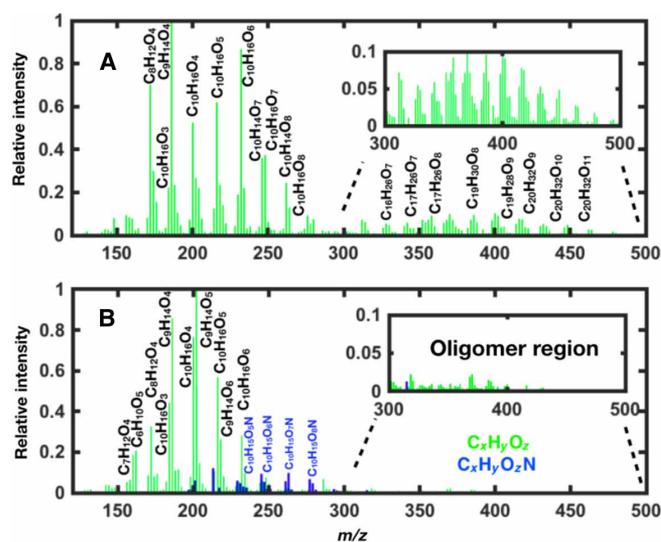

Fig. 1. Mass spectral comparison of laboratory and ambient organic aerosol. (**A**) Mass spectrum (30-s average) of all secondary aerosol compounds generated during an α-pinene ozonolysis experiment in the atmospheric simulation chamber at the Paul Scherrer Institute, measured by the EESI-TOF at a mass loading of ~23 μg m^{-3} (**B**) Mass spectrum (30-s average) of all compounds measured by the same instrument in the particle plume observed in Hyytiälä with total mass loadings of ~14 μg m^{-3} (see fig. S1). An expanded view of the oligomer region (300 to 500 m/z) is shown in the upper right corner. The signal is normalized to the maxima of the highest organic peaks observed ($C_9H_{14}O_5$ for Hyytiälä and $C_9H_{14}O_4$ for the chamber study). Corresponding mass defect plots for these two spectra are shown in fig. S2.

hours and were also reported in previous studies (21, 22). Last, the dimer formation from α-pinene may be more efficient than the ambient monoterpene ensemble due to structural differences, e.g., endocyclic position of the double bond (17).

These differences between the smog chamber and ambient SOA are interesting; however, the salient feature of Fig. 1 is the extensive overlap of molecules measured in both the chamber and the field. Depending on concentration, ~80 to 88% of the signal in Hyytiälä corresponds to ions observed in our chamber study. The remaining signal is attributed primarily to organonitrates, as ~6 to 13% of the nonoverlapping signal comes from the nitrogen-containing ions discussed above, and ~4% from C_{11}–C_{14} molecules, which may be either small dimers or sesquiterpene products. The remaining signal constitutes less than 1%. Likewise, 65% of the total signal found in the chamber corresponds to ions identified in Hyytiälä, with only 2% of the signal attributed to monomers not found in Hyytiälä. For the reasons identified above, most differences occur in the dimer region; 28% of the nonoverlapping chamber signal is attributed to C_{16}–C_{20} dimers and 4% to C_{11}–C_{15} dimers. The strong similarity of the chamber mass spectrum to the Hyytiälä measurements (discussed above) and, to a lesser extent, to a factor related to monoterpene oxidation retrieved from source apportionment of OA in Zurich (23) suggests that the overall aerosol composition is likewise similar, and therefore, the reactive processes observed in the chamber are highly likely to occur also in the atmosphere. Establishing a quantitative relationship between reactions observed in the chamber and those in ambient air (where conditions also vary considerably) is, of course, very challenging, and not attempted here. Among other factors, the presence of NO_x in the atmosphere (even at the Hyytiälä site) and/or higher concentrations of HO_2 radicals compared to chamber

experiments will alter the fate of the RO_2 radicals in the gas phase and therefore the particle-phase composition.

Figure 2 (A and C) compares the time series of $C_{20}H_{32}O_{10}$, $C_{17}H_{28}O_{9/10}$, and $C_{10}H_{16}O_8$ in the gas phase measured by the nitrate CIMS (as well as α-pinene from the PTR-TOF-MS) and particle phase measured by the EESI-TOF. In the gas phase (Fig. 2A), each of these three products (one monomer and two dimers) is formed directly after the α-pinene injection and rapidly depletes to near-zero concentrations within ~20 min. This is consistent with their high carbon and oxygen numbers, and thus low volatilities, promoting rapid new particle formation and irreversible condensation onto preexisting surfaces (particles and chamber walls) (*4*). Similar behavior is seen for other gas-phase HOM dimers, as shown in fig. S3. While these example molecules have approximately the same temporal patterns in the gas phase, their evolution in the particle phase is very different (Fig. 2C). Specifically, the $C_{10}H_{16}O_8$ monomer and the $C_{20}H_{32}O_{10}$ dimer immediately partition into the particle phase, reach a maximum signal after 20 to 40 min, and then steadily decay. In contrast, the $C_{17}H_{28}O_9$ dimer peaks concurrently with the above compounds but decays more slowly, whereas $C_{16}H_{24}O_8$ reaches its maximum intensity only after ~3 hours and does not decay significantly thereafter. It should be noted that >90% of α-pinene has reacted already after 1 hour. Therefore, the different particle-phase time trends suggest that particle-phase processes can substantially affect the formation and transformation of HOM species.

Figure 2 (B and D) displays the time evolution of particulate dimers and monomers, respectively, represented as the summed signal of all ions with the same carbon number. Figure 2B shows a faster decay of dimers containing more carbon (especially C_{20}

molecules) than those with lower carbon number. This behavior cannot be explained by evaporation. The C_{20} compounds in our study contain 6 to 15 oxygen atoms, corresponding to saturation vapor concentrations (C*) of about 10^{-7} to 10^{-15} μg m^{-3} based on a group contribution method (fig. S5) and comparable to a previous study (*24*). These saturation vapor concentrations are too low for evaporation to be significant. Further, evaporation would be expected to yield the opposite trend from that observed, with the heavier C_{20} molecules remaining longer in the particle phase. A similar trend is evident in the monomer region (C_6–C_{10}; Fig. 2D), with molecules containing more carbon atoms (especially C_{10} compounds) decaying more rapidly in the particle phase than molecules with less carbon atoms. In this monomer region, the saturation vapor concentration of the molecules is estimated to be between 10^{-4} and 10^3 μg m^{-3}, and therefore, evaporation could affect the evolution of the more volatile species in the particle phase. However, like the dimers, evaporation would preferentially remove molecules with less carbon, thus actually acting in opposition to the observed trends. Further, within the very broad span of volatilities (logC* ~10^{-15} to 10^3 μg m^{-3}) for the measured ions, we do not observe correlation between the signal remaining after 12 hours and the saturation vapor concentration (fig. S6). Together, these observations exclude evaporation as a main removal process.

The signal of C_{16}–C_{17} compounds in Fig. 2B peaks, on average, 2 hours later than the C_{20} compounds. On the basis of current knowledge, dimers can be formed in the gas phase via RO_2· + RO_2· chemistry or reactions between Criegee intermediates and carboxylic acids (*25*). These reactions would happen immediately after the initiation of α-pinene oxidation due to the high reactivity of both
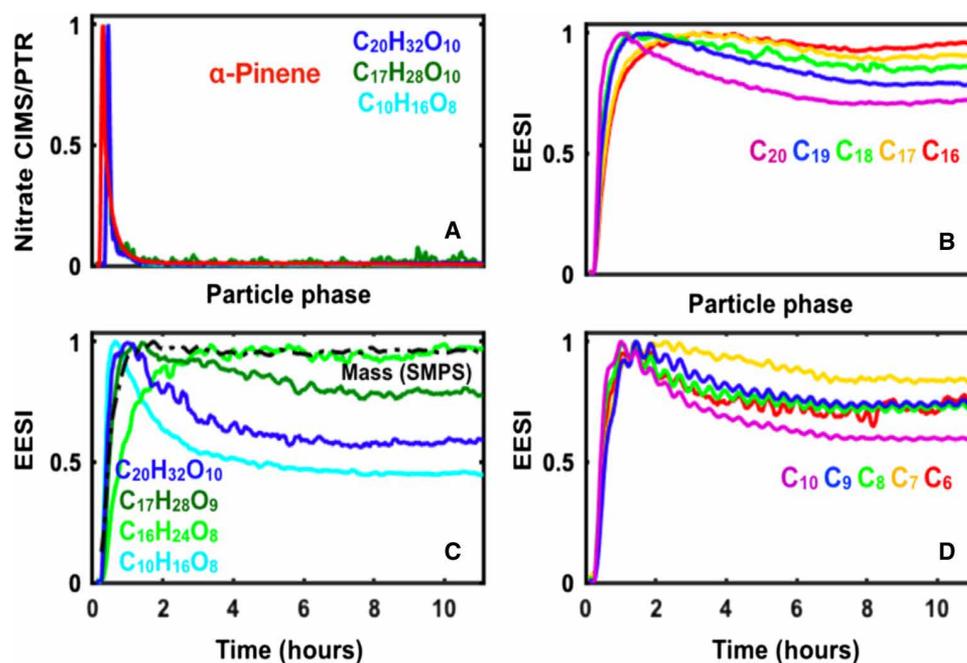

Fig. 2. Time evolution of particle and gas-phase composition for α-pinene ozonolysis. (**A**) α-Pinene injection into the chamber (~35 ppbv) measured by the PTR-TOF-MS and gas-phase evolution of its oxidation products measured by the nitrate CIMS. The measured highly oxygenated molecules show fast production and immediate depletion from the gas phase due to their low volatility. (**B**) Time evolution of particle phase dimers, grouped by their carbon number. (**C**) Time evolution of three dimers and one monomer measured in the particle phase showing very distinct behavior despite similar saturation vapor concentrations. (**D**) Time evolution of particle phase monomers, grouped by their carbon number. All signals are normalized to the maximum signal recorded for the respective ion during the displayed period. All data are taken from experiment 1, except for α-pinene, which is taken from experiment 2 (which has similar initial conditions; see table S1) due to nonavailable PTR-TOF-MS data.

Criegee and $RO_2\cdot$, and these dimers with very low volatility are expected to partition to the particle directly after their gas-phase production. This is seen for most C_{18-20} dimer species. However, the later time of signal maximum for C_{16-17} (2 to 3 hours) in the particle phase indicates that formation processes other than gas-phase oxidation play a substantial role. No further reactions in the gas phase are expected to occur after the consumption of α-pinene because, by then, the OH· radicals, produced by the decomposition of carbonyl oxides formed via α-pinene ozonolysis, are depleted. Also, none of the gas-phase species measured by the nitrate CIMS exhibit substantial delay in their maxima (see Fig. 2A and fig. S3). Therefore, we propose that these dimers are strongly affected by particle-phase chemistry, likely involving the combined effects of both accretion reactions ($C_{7-10} + C_{7-10} \rightarrow C_{14-20}$) and the decomposition of higher–molecular weight compounds ($C_{20} \rightarrow C_{16-19}$). These reactions would then also contribute to the observed decays of C_{8-10} and/or C_{20} species.

Accretion reactions transform the mass from monomers to oligomers, yielding products with a higher number of carbon atoms and converting semivolatile molecules into higher–molecular weight compounds with lower saturation vapor concentrations. These reactions have been studied under laboratory conditions and suggested to play an important role in ambient environment (26–28). Accretion reactions will increase the persistence of organic mass in the particle and enhance the growth rate to CCN-relevant sizes (29). In our case, if accretion reactions contributed substantially to the monomer decay, then the dimer:monomer ratio would increase as the experiment progresses, and dimers would reach their maximum concentration later than the corresponding monomers. This ratio would be further increased by monomers of sufficiently high vapor concentrations repartitioning to the gas phase, resulting in net mass loss from the particles. However, the wall loss–corrected SOA mass peaks 1 hour after α-pinene injection and thereafter shows only a slight decrease. Figure 3 shows the fractional contributions to the total EESI-TOF signal intensity for measured compounds classified as monomers (C_5–C_{10}) or dimers (C_{15}–C_{20}). Over the course of 12 hours, the dimer fraction increases only from 27 to ~35%. This relatively constant dimer:monomer ratio suggests that accretion reactions likely cannot explain the observed compositional changes and that these reactions are slow relative to the investigated experimental time scales. Alternatively, if dimer formation were to shift the gas/particle equilibrium of monomers, replenishing the particle-phase monomers and buffering the monomer:dimer ratio, a net increase of organic mass would result, instead of the decay of both monomers and dimers
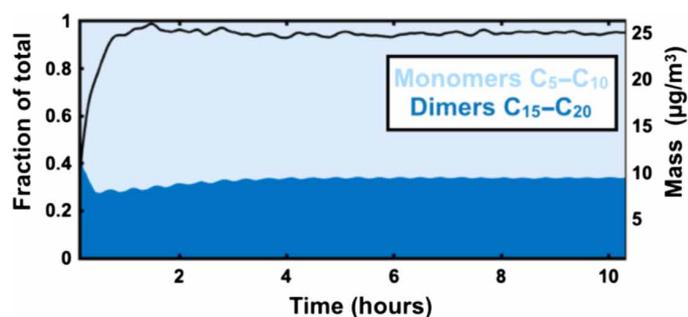
that is actually observed. Therefore, the observed dynamics are most likely due to the compounds' decomposition in the particle phase.

Further insights into the production and decomposition processes in the particle phase are obtained by the investigation of the temporal behavior of individual molecules. Figure 4 shows the mass defect plots [exact mass/charge ratio (m/z) minus nearest integer versus m/z] for all particle-phase ions, color-coded by the time of maximum signal (Fig. 4A), decay rate after reaching the maximum signal (Fig. 4B), and the fraction of signal remaining after 12 hours relative to maximum (Fig. 4C); decay rates and remaining signal are also reported for selected ions in table S2. Decay rates are determined from an exponential fit beginning after the ion reaches its maximum signal (fig. S7). For reasons discussed later, most ion signals do not decay to zero; the exponential fit therefore includes a y offset (i.e., $y = y_0 + Ae^{-kt}$), and we define the half-life as the time required for the signal to decay to $(y_{max} - y_o)/2$. Symbol area denotes the square root of ion signal at the time of maximum total aerosol mass. Figure 4A exhibits the same general trends as discussed earlier in conjunction with Fig. 2 (i.e., consistent with particle-phase reactions yielding products with lower carbon number); however, substantial differences between specific ion groups are evident. The highly oxygenated $C_8H_{12}O_x$, $C_9H_{14}O_x$, and $C_{10}H_{16-18}O_x$ compounds appear first in the particle phase followed by less oxygenated $C_{8-10}H_{12-16}O_x$, which is consistent with the partitioning behavior of these compounds, as the compounds' saturation vapor concentration increases with decreasing number of oxygen and more volatile compounds are expected to condense later. However, this trend contrasts with the trend of decreasing carbon number discussed above, suggesting that the monomer composition may be influenced by both partitioning and particle-phase decomposition reactions.

As shown in Fig. 4B, $C_{20}H_{32}O_x$ dimers and $C_{10}H_{18}O_x$ monomers have the fastest decay rates, exceeding 20×10^{-3} min^{-1}. A similar trend for the $C_{10}H_{18}O_x$ ions is also observed by FIGAERO, as shown exemplarily for two C_{10} species in fig. S8. Most $C_{10}H_{18}O_x$ and $C_{20}H_{32}O_x$ are expected to come from oxidation of α-pinene by OH· that is formed during ozonolysis via the decomposition of Criegee intermediates. In fig. S9, the time series of $C_{10}H_{18}O_{4-8}$ and $C_{20}H_{32}O_{6-10}$ for experiments with and without OH· scavenger are shown. Clearly, in the OH scavenger experiment, the absolute signal of these molecules is much lower, with the exception of $C_{10}H_{18}O_4$ and $C_{20}H_{32}O_6$. Therefore, the most unstable HOMs observed in this study likely result primarily from the OH-driven autoxidation pathway.

A few specific ions have decay rates of 5×10^{-3} to 15×10^{-3} min^{-1}—i.e., $C_9H_{16}O_{5-8}$, $C_9H_{14}O_5$, and $C_8H_{12}O_{7-8}$—corresponding to half-lives of ~60 to 200 min. These decay rates are of the same order as the total peroxide decay rates in SOA from α-pinene ozonolysis (16×10^{-3} min^{-1}) measured by spectrophotometric iodometry (2 hours after particle collection) (30). Reactive oxygen species (ROS) such as peroxides are rapidly formed in the gas phase by autoxidation and comprise a substantial fraction of secondary aerosol mass (31, 32). In a similar study focusing on the oxidation of limonene by ozone, a significant particle-phase decay was reported for $C_{10}H_{16}O_4$, a major product of limonene ozonolysis (33). However, some of limonene's oxygenated products (like $C_{10}H_{16}O_4$) still contain an intact exo C=C bond available for further reaction with ozone, which may also explain the observed particle-phase decrease of that species. In contrast, α-pinene loses its single double bond in the first oxidation step; therefore, its oxygenated products do not further react with the excess ozone present in the chamber. The decay rates are
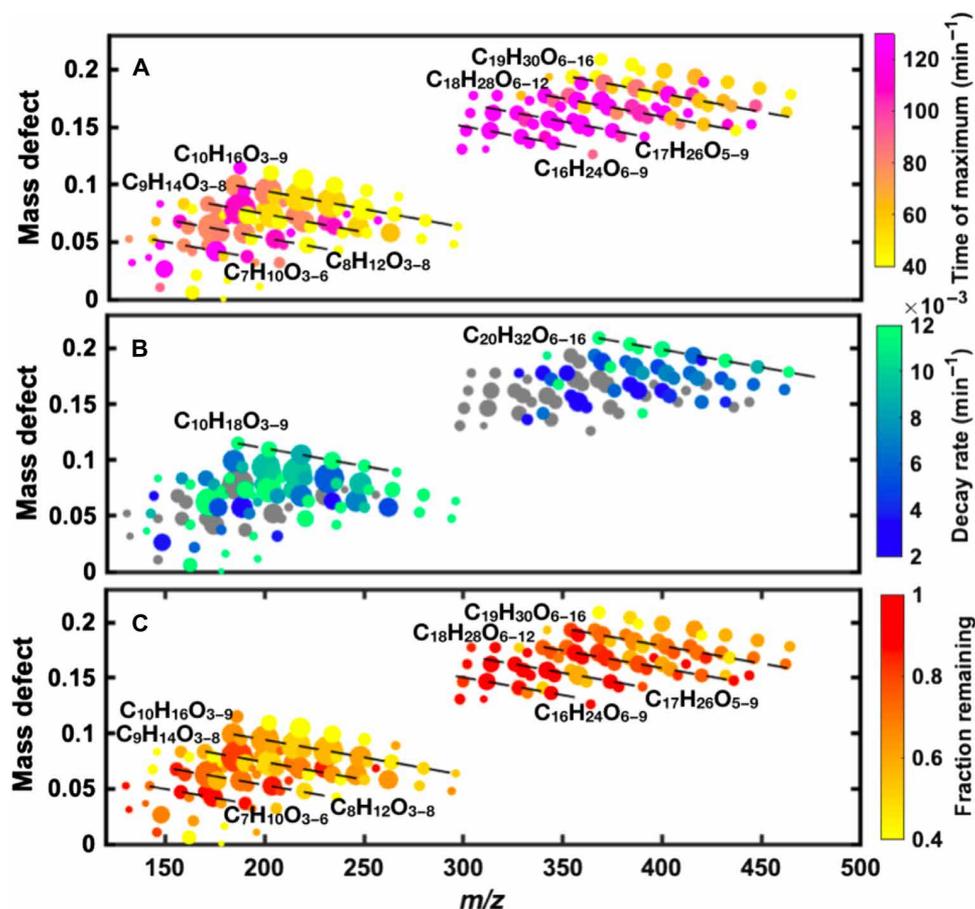

Fig. 3. Relative monomer (C_5–C_{10}) and dimer (C_{15}–C_{20}) fraction measured by the EESI-TOF to the total signal (sum of all monomers and dimers) for chamber experiment 1. The right axis shows wall loss–corrected mass measured by the SMPS.

Fig. 4. Mass defect plot of species detected by the EESI-TOF in the SOA produced by α-pinene ozonolysis (experiment 1). Mass defect plot of species detected by the EESI-TOF in the SOA produced by α-pinene ozonolysis (experiment 1) color-coded by (**A**) time of the maximum signal of the respective particle-phase species, (**B**) individual decay rate of each species (dark gray markers correspond to ions that do not show any decay in the particle), and (**C**) fraction of remaining signal after 12 hours (after wall loss correction). Symbol areas are sized according to the square root of ion signal at the time when the maximum mass was reached in the chamber.

also similar to the hypothesized decomposition rates for reversibly formed oligomers (defined as oligomers that decompose in response to heat or time, yielding volatile monomers) in the isothermal evaporation of α-pinene SOA. This process was proposed by D'Ambro *et al.* (*34*) to explain the observed composition and volatility changes of the SOA particles with time. Oligomer decomposition and/or other volatility-increasing chemical reactions were suggested, controlling the early stages of the SOA evolution. The reported values for oligomer decomposition rates were between 6×10^{-3} and $6 \times 10^{-4} \, \mathrm{min}^{-1}$ (*34*). The observed decay rates in our study and D'Ambro *et al.* (*34*) are in good agreement; however, our results strongly suggest fragmentation reactions of both monomers and dimers toward molecules with lower carbon number. We do not have supporting evidence for solely the decomposition of reversible oligomers into their volatile monomer species as the driving force of early SOA aging. As shown in Fig. 3, we do not observe significant changes in the relative ratios of monomer versus dimer concentrations.

It is important to note that the decay stops or greatly slows down after ~6 to 7 hours depending on the species considered (fig. S7). One hypothesis for this could be a change in the physicochemical properties of the aerosol, such as increased viscosity due to particle-phase reactions. The viscosity of α-pinene SOA has been extensively studied, with a wide range of values obtained depending on experi-

mental conditions. For example, the viscosity of an α-pinene SOA system at ~40% RH lies in the range of ~10^5 to $10^7 \, \mathrm{Pa \, s}^{-1}$ and can increase by orders of magnitude with atmospheric aging (*35*). This corresponds to a semisolid phase state where certain reactions can be diffusion-limited, therefore potentially hindering bi- or multimolecular particle-phase reactions (whereas no effect is expected on unimolecular reactions). Although the diffusion of relevant organic molecules in α-pinene SOA is poorly constrained, the diffusion of water molecules was shown to not be kinetically limited for atmospheric-sized particles (*36*), whereas the diffusion of NH_3 into α-pinene SOA is limited below 30 to 40% RH (*37*). The uncertainties in SOA diffusion coefficients prevent us from fully ruling out this effect; however, if the aerosol did become sufficiently viscous to shut down the particle-phase reactions, one would expect a simultaneous termination of the decay of all ions independent of their composition, which is not observed here (e.g., Fig. 2C).

Another explanation for the termination of particle-phase decomposition reactions is the presence of isomers of different reactivity/stability in the particle. Once the reactive molecules are consumed, the particle-phase reactions would end. Similar conclusions can be made from Fig. 4C, where the fraction of the remaining signal after 12 hours is shown. The C_{20} dimers and $C_{10}H_{18}O_x$ show the highest signal loss, corresponding to ~30 to 40% of their maximum

values. In contrast, no significant loss of C_{16} or C_{17} ions is observed. This observation shows that the particle-phase chemistry causes changes in the overall SOA composition over the time scale observed here.

The decay shown in Fig. 4 is ubiquitous throughout the spectrum, with a 20% decrease in signal occurring for 78% (71 of 91) of monomers and 56% (71 of 127) of dimers. Of the ions exhibiting this decay, 78% have half-lives of less than 120 min (87% of monomers and 69% of dimers), while 46% have half-lives of less than 60 min (58% of monomers and 35% of dimers). These time scales are similar to or faster than typical aerosol collection times for semicontinuous or offline measurement techniques, suggesting that substantial changes in composition may occur even while the aerosol is being collected. For example, the FIGAERO-I-CIMS particle module operated with a 40-min collection cycle followed by a 40-min desorption cycle, while recent attempts to assess aerosol peroxide content included collection times ranging from 45 min (*38*) to 15 to 18 hours (*39*). In this latter case, SOA from α-pinene ozonolysis was continuously generated in a flow tube and deposited on a filter; offline analysis indicated near-zero concentrations of large peroxides, which our results suggest is likely because of decomposition reactions on the filter. Further, most experiments relying on offline analyses use much longer delays between collection and analysis (although refrigeration of collected samples likely somewhat slows reaction). However, these rapid and ubiquitous reactions highlight the limitations of traditional offline techniques for the investigation of aerosol composition, reactions, and kinetics. Therefore, we exploit the previously unavailable real-time composition data from the EESI-TOF to obtain further insight into the potential mechanisms and atmospheric implications associated with these particle-phase reactions.

DISCUSSION

Several mechanisms have been proposed to explain the decay of secondary aerosol species. Zhang *et al.* (*40*) proposed decarboxylation of diacylperoxides, leading to the formation of new covalently bound ester accretion products. This reaction results in the loss of CO_2, with a corresponding decrease of the O:C ratio. In the experiments presented here, the O:C ratio does not decrease sufficiently (from 0.54 to 0.51), as a loss of CO_2 would suggest. Kahnt *et al.* (*41*) explained the presence of two high–molecular weight esters ($C_{19}H_{26}O_7$ and $C_{17}H_{26}O_8$) through the decomposition of $C_{19}H_{28}O_{11}$ with loss of oxygen or a ketene from the inner part containing a labile trioxide function, and the conversion of the unstable acyl hydroperoxide groups to carboxyl. In Fig. 5A, we show the time evolution of these species. The parent molecule ($C_{19}H_{28}O_{11}$) rapidly reaches a maximum and then shows a continuous decay in the particle phase, and the esters appear at a later stage. However, considering the much higher absolute signals of the esters compared to the proposed parent molecule (0.001 ag s^{-1} for $C_{19}H_{28}O_{11}$, 0.104 ag s^{-1} for $C_{19}H_{28}O_7$, and 0.144 ag s^{-1} for $C_{17}H_{26}O_8$) and the fact that we do not expect large discrepancies in terms of sensitivity for these species, we conclude that this is likely not the major formation pathway of these esters. A recent study by Claflin *et al.* (*42*) revealed large discrepancies between the observed groups and those predicted by the Master Chemical Mechanism (MCM) based on the functional group analysis of α-pinene SOA collected on filter samples. Specifically, peroxides, peroxyacids, aldehydes, and ketones were overpredicted, while esters and acids were larger than expected. Baeyer-Villiger reactions were suggested

as a possible reaction pathway, where carboxylic acids and esters can be formed from the aforementioned species. This form of reaction seems to be more consistent with our observations and is discussed further below.

In Baeyer-Villiger reactions, a peroxyacid or hydroperoxide oxidizes a ketone or aldehyde to an ester or acid, respectively, while the peroxyacid or hydroperoxide is converted to an acid, alcohol, or ketone. The conversion of a hydroperoxide to a ketone yields a net loss of H_2. This agrees with the trend observed in Fig. 5B, where the time evolution of C_{10} monomers grouped by hydrogen number is shown. The monomers with the highest number of hydrogens peak first in the particle phase and decay faster than the less hydrogenated monomers. More specifically, the conversion of $C_{10}H_{18}O_x$ to a ketone through Baeyer-Villiger reaction would cause its decrease in signal and net loss of H_2O generating a compound with the formula $C_{10}H_{16}O_{x-1}$ and explain delayed peaks of the less hydrogenated species in the particle. In Fig. 5 (C and D), we show $C_{10}H_{18}O_6$ and $C_{10}H_{16}O_8$ as example molecules that could decay through Baeyer-Villiger reactions contributing to the production of $C_{10}H_{16}O_5$ and $C_{10}H_{14}O_7$, respectively, after a formal loss of H_2O (note that the
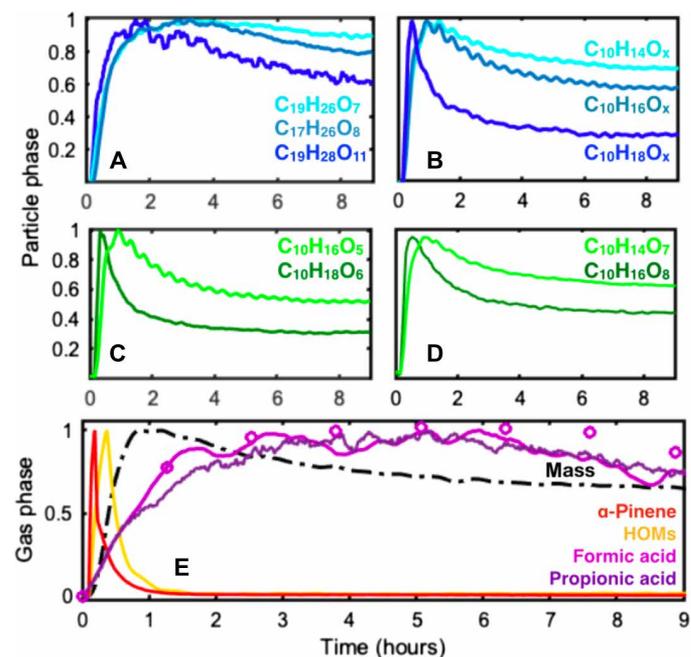

Fig. 5. Time evolution of selected particle and gas-phase species measured during an α-pinene ozonolysis experiment. (**A**) Time evolution of three dimer species in the particle phase measured by EESI-TOF. (**B**) Time evolution of $C_{10}H_{14–18}O_x$ monomers in the particle grouped by their number of hydrogens. (**C** and **D**) Time evolution of $C_{10}H_{18}O_6$ and $C_{10}H_{16}O_8$ species and their potential decomposition products $C_{10}H_{16}O_5$ and $C_{10}H_{14}O_7$. The decay rates of ~0.01 to 0.02 min^{-1} correspond to the lifetimes of about 50 to 100 min. The potential decomposition products $C_{10}H_{16}O_5$ and $C_{10}H_{14}O_7$ correspond to possible reduction of the hydroperoxide group to a ketone group. (**E**) PTR-TOF-MS gas-phase measurement of α-pinene (red) and total signal of HOMs measured by the nitrate CIMS (orange). Formic acid (magenta) is measured simultaneously by the PTR-TOF-MS and the iodide CIMS (circles) in the gas phase, with substantial delay suggesting its secondary formation due to decomposition reactions. Propionic acid (or an isomer corresponding to $C_3H_6O_2$ such as hydroxyacetone or methylacetate) is observed with similar time evolution. Signal of each molecule is normalized to the maximum signal recorded for the respective ion during the displayed period.

product molecules likely have other formation pathways in addition to the Baeyer-Villiger reaction). $C_{10}H_{18}O_x$ ($x > 4$) are mainly a product of OH· oxidation (fig. S9) and, via the Baeyer-Villiger reaction, would not have an additional source, which might explain their faster decay and earliest peak in the particle relative to the other molecules.

In addition, the observed kinetics for individual particle-phase oxygenated species are consistent with the Baeyer-Villiger reaction. Alvarez-Idaboy et al. (43) reported second-order rate constants of 0.108 and 19.2 M^{-1} min^{-1} (303 K) for the trifluoroacetic acid–catalyzed reaction in dichloromethane of trifluoroperacetic acid with propanone and cyclohexanone, respectively. Taking these rate constants as boundary conditions, the fastest decay rates observed in the current study (about 20×10^{-3} min^{-1}) would require bimolecular reaction partner concentrations of 1.0×10^{-3} to 0.19 M, which, assuming an aerosol density of 1.2 g cm^{-3} and a mean molecular weight of 200 g mol^{-1}, correspond to 0.017 to 3.1% of the SOA mass. Although an imperfect model for the SOA system, these Baeyer-Villiger kinetics are likely fast enough to explain the observed decay rates and roughly consistent with our observations.

The hydrolysis of esters, formed by the Baeyer-Villiger reactions, would further produce small volatile molecules (C_1–C_3), which, despite their high volatility, have been found in aerosol filter samples (10), consistent with the observed loss of carbon and the formation of lower carbon number molecules (C_7–C_9 and C_{16}–C_{17}) in the particle with increasing time (Fig. 2). The evolution of small oxygenated molecules, released during these particle-phase reactions as decomposition byproducts, can also be observed in the gas phase. Figure 5E shows the time series of gas-phase formic acid (~3 to 4 ppbv) and propionic acid [~600 parts per trillion by volume (pptv)] for experiment 4. The maximum signal of these acids is observed well after α-pinene is depleted in the gas phase and with substantial delay relative to both the nitrate CIMS HOMs in the gas phase and the peak of the particle mass. Formic acid and/or other low–molecular weight carbonyls/ketones have been reported previously during photo-oxidation experiments of monoterpenes, where these molecules were attributed to gas-phase photooxidation reactions (44, 45). A more recent study observed a similar trend for small acids and carbonyls from the ozonolysis of limonene, where this was explained by secondary OH-mediated fragmentation of the limonene backbone (33). However, the present study was conducted without lights, and the production of these acids cannot be explained solely by OH· chemistry, as their time scale is unaltered by the addition of an OH scavenger (fig. S10). Instead, the gas-phase acid trend is consistent with the decrease in carbon number for particle-phase monomers and dimers (Fig. 2, B and D) and thus is likely linked to particle-phase reactions.

Besides the abovementioned hydrolysis of esters, the Korcek mechanism could also explain these gas-phase observations. This mechanism involves the formation of a cyclic peroxide between a carbonyl and a hydroperoxide group, followed by the cleavage of the O—O and C—C bonds, leading to the formation of an acid and an aldehyde (46). Carbonyl and hydroperoxide groups are ubiquitous in organic molecules formed through autoxidation, and the formation of cyclic peroxides (more specifically peroxyhemiacetals) has been reported previously (32). These, apart from the Korcek mechanism, can be transformed further through different pathways (37) and cause the decomposition and lack of hydroperoxide-OOH moieties observed in the aged aerosol sample (10, 30, 39). Although Korcek mechanism kinetics have not been studied at typical atmospheric temperatures, a decay rate of 2.7×10^{-3} min^{-1} was observed at 393 K

(46). This falls in the range of the typical decay rates observed here, although direct comparisons are complicated by (i) the ~100 K higher temperatures in the laboratory experiment, which increases the reaction rate, and (ii) possible reactivity differences between the α-pinene system studied here and the hexadecane system for which the Korcek mechanism kinetics have been studied. Our findings provide the first molecular-level evidence for intraparticle hydroperoxide decomposition reactions and confirm that these reactions occur very rapidly, altering the SOA composition. However, the absence of direct structural information hinders confirmation of the dominant chemical mechanisms and highlights the need for continued progress toward online molecular characterization of SOA.

The experimental evidence discussed here demonstrates that particle-phase reactions have an important impact on the evolution of SOA. These reactions are likely driven by the consumption/decomposition reactions of particle-phase ROS, such as hydroperoxides, peroxides, and peroxyacids, which are thought to be associated with adverse health effects of particulate matter (47) and thus of high interest. We measured their decays in the particle phase for the first time on a quasi-molecular level and observed lifetimes of about 30 to 150 min, consistent with previous findings on short-lived, nonspeciated ROS measured by acellular assays (30, 33). Once the ROS species are consumed, no further significant changes of the SOA composition on the time scale of our experiments (~12 hours) are observed. This would mean substantially less ROS in aged air masses relative to the air masses with freshly formed SOA. It also highlights the importance of real-time measurements for the accurate measurement of ROS, as the reactions during and after sample collection affecting longer–time scale offline techniques may lead to an underestimate of ROS and its associated health effects. Likewise, experiments focusing on near-source ROS measurements may overestimate health effects unless ROS decomposition is accounted for. In our experiments, substantial decay is exhibited by the vast majority of measured ions, indicating that they include at least one ROS isomer. The rapidity and ubiquity of these reactions highlight the importance of real-time measurements for compositional and mechanistic studies (even without complete molecular identification), as the obtained kinetic parameters provide a crucial complement to traditional analyses focusing on structural identification.

Further, with aerosol aging, we observe the formation of small volatile carboxylic acids that partition irreversibly to the gas phase. Formic acid is the most prominent, with a yield of 5 to 7%. Note that in our experiments, formic acid is predominantly generated from intraparticle reactions given its strong temporal correlation with these processes, and to our knowledge, no mechanism for dark multigenerational gas-phase production of formic acid has been proposed. Large discrepancies between measured and modeled concentrations of formic acid are often reported, suggesting an underestimation of formic acid fluxes in models (48, 49). Recent measurements in a boreal environment showed that the measured fluxes of formic acid are one order of magnitude higher than estimated from direct soil and vegetation emissions or from secondary production from terpene oxidation (50). Here, we show that formic acid yields from particle-phase reactions are comparable to those from terpene oxidation in the gas phase [assumed to be ~10% in (51)]. This signifies that this source may contribute another 10% of the total measured flux in the boreal forest. This hypothesis is based on the assumption that SOA from other terpene systems produces formic acid with the same yields, which should be verified in future

studies. On a global scale, with 95 Tg year^{-1} of monoterpene emissions, we estimate that the particle processing of monoterpene SOA would lead to an additional source of formic acid of 4.7 to 6.6 Tg year^{-1}. This is comparable to the primary emissions of 3.5 Tg year^{-1} currently estimated by global models (e.g., MEGAN) (48). This suggests that the contribution of intraparticle reactions to global formic acid concentrations may be substantial although the formic acid source proposed here is considerably smaller than the ~46 Tg year^{-1} of formic acid estimated to derive from unknown sources (49). However, other SOA moieties containing peroxides or other labile molecules may follow similar chemical pathways. The estimates provided above should therefore be considered as a lower limit to the total formic acid production from HOM decomposition. Although these reactions may not fully explain the missing formic acid sources, their magnitude indicates that particle-phase reactions have implications not only for the SOA composition but also for the overall global budget of formic acid.

MATERIALS AND METHODS

Chamber and experimental description

The dark ozonolysis of α-pinene was studied through a sequence of experiments performed in an environmental reaction chamber located at the Paul Scherrer Institute (50). The chamber consists of a 27-m^3 bag made of fluorinated ethylene propylene in a temperature-controlled wooden enclosure maintained at 22°C. Clean air is provided by an air purifier (737-250 series, AADCO Instruments Inc.). The chamber was operated in batch mode with a minor dilution flow of purified air at ~30 liters min^{-1} to maintain the chamber volume despite continuous sampling by all instruments. Because of this extra dilution, the residence time in the chamber was 15 hours. Before each experiment, the chamber was cleaned by flushing pure air and water vapor to set it to 40 to 50% RH. Next, 400 ppbv of O$_3$ was injected and allowed to mix. Last, α-pinene (5 μl) was injected through a septum into a thermally isolated heated glass tube, which was subsequently flushed for 30 s by purified air into the chamber. Because the concentration of O$_3$ was in excess relative to α-pinene, HOMs of low volatilities were rapidly formed, inducing new particle formation and growth by condensation of SOA. This rapidly increased the particle-phase condensational sink and reduced the loss of oxidized vapors to the chamber walls.

Wall loss correction

The mass measured by the SMPS and each EESI-TOF ion signal were corrected for wall loss using the dynamic wall loss rate (k_{wall}). k_{wall} is based on the exponential decay of the particle number concentration, which has been corrected for coagulation following Eq. 1, where N corresponds to the particle number concentration and k_{coag} corresponds to the coagulation coefficient. The equation was fitted near the end of the experiment, after particle production had ceased. No correction was applied for partitioning of semivolatile species to the chamber walls.

$$\frac{dN}{dt} = -k_{coag} * N^2 - k_{wall} * N \qquad (1)$$

Extractive electrospray ionization time-of-flight mass spectrometry

The chemical composition of SOA was measured online with a novel EESI-TOF (13). The EESI-TOF consists of a homebuilt EESI inlet coupled to an atmospheric pressure interface time-of-flight mass spectrometer (Tofwerk AG). Particles are sampled at a flow rate of ~0.8 liters min^{-1} through an extruded carbon denuder into a plume of charged droplets generated by passing solvent through a conventional electrospray probe. The collision between sampled aerosol and produced electrospray droplets results in the extraction of the soluble components of the aerosol. The charged droplets are then gently evaporated, yielding ions via Coulomb explosion, which are then sampled directly into a mass spectrometer. The electrospray working solution consists of 1:1 water:methanol doped with 100 ppm NaI. Positive ion spectra are recorded at 1 Hz. For aerosol components, the NaI additive suppresses virtually all ionization pathways other than adduct formation with Na$^+$. This contributes to an instrument response that is linear with mass for all ions and unaffected by a changing organic matrix. Figure S11 shows the total EESI-TOF signal as a function of SMPS mass and surface for a sample experiment, showing a tight linear correlation and indicating that the bulk EESI-TOF sensitivity does not significantly vary in response to the chemical evolution of the measured SOA. We report the EESI-TOF signal in terms of the mass flux of ions reaching the microchannel plate detector in the mass spectrometer. This is calculated as the product of the measured signal (ions per second) and the molecular weight of the respective ion (excluding the attached Na$^+$) and is reported in attograms per second. Aside from the Na$^+$ attachment, no formation of noncovalently bound adducts (e.g., noncovalent dimers) was observed. This was confirmed by comparison of the EESI-TOF mass spectra with chemical ionization instruments (FIGAERO-I-CIMS and nitrate CIMS described below) and by declustering scans performed by ramping the collision energy within the ion transfer optics.

Other instruments

Several other mass spectrometers and supporting instruments were used to monitor the gas-phase composition. The concentration of α-pinene was measured with a PTR-TOF-MS (Ionicon Analytik) (52). Oxidation products were measured with a nitrate CIMS (Airmodus) and a high-resolution time-of-flight iodide CIMS coupled to a filter inlet for aerosol and gases (FIGAERO-I-CIMS, Aerodyne Research Inc.) (18). Both instruments measure the gas phase, with the nitrate CIMS preferentially detecting more highly oxygenated molecules, while the FIGAERO-I-CIMS additionally measures particle composition as discussed below. The nitrate CIMS was operated at a standard total flow of 30 liters min^{-1}, with 20 liters min^{-1} sheath flow connected to the chamber with a 0.75-inch tube. The FIGAERO-I-CIMS sampled the gas phase at 6 liters min^{-1} through a 200-cm-long Teflon tube with 0.6 cm inner diameter (ID). Both instruments used an ion source (x-ray generator) to ionize the reagent gas in a nitrogen flow. The FIGAERO-I-CIMS additionally provides a semicontinuous measurement of SOA composition with a time resolution of 40 min as follows. Particles were collected on a Teflon [polytetrafluoroethylene (PTFE)] filter after passing through a 200-cm stainless steel tube with 0.4 cm ID at 5 liters min^{-1}. After collection, organic molecules were desorbed by a flow of nitrogen that is gradually heated from room temperature to 200°C over the course of 40 min. The resulting signal as a function of desorption temperature (thermogram) was integrated to determine the total signal corresponding to a given ion across the entire collection period. The concentration of O$_3$ was measured with an Environics S300 ozone analyzer and a Monitor Labs 8810 ozone analyzer. The particle volume distribution was continuously monitored with an

SMPS. For conversion to mass, an effective density of 1.2 g cm^{-3} was assumed.

Ambient measurements

Field measurements were performed at the SMEAR II station in Hyytiälä, Finland. The measurement site is located in the Finnish boreal forest, and particle nucleation and growth events strongly influenced by the monoterpene oxidation products are frequently observed (53). The EESI-TOF was sampled from a permanent ground-based measurement container together with a quadrupole aerosol chemical speciation monitor (Q-ACSM; Aerodyne Research Inc.) and differential mobility particle sizer. These instruments were measured with 1-s, 3-min, and 30-min time resolution, respectively. Major ion signals from the EESI-TOF generally matched the time series of organic mass measured by the Q-ACSM (see fig. S1). This illustrates the linear performance of the instrument and the ability to reliably measure SOA components with high time resolution even at the low concentrations present in remote locations.

SUPPLEMENTARY MATERIALS

Fig. S1. Real-time particle measurement in Hyytiälä.
Fig. S2. Wind directions above the canopy and organic mass measured by the ACSM in Hyytiälä.
Fig. S3. Similarity scores between the α-pinene ozonolysis and ambient Hyytiälä mass spectra from the current study (see Fig. 1) with each other as well as with EESI-TOF mass spectra from source apportionment of summer measurements in Zurich (23) and from laboratory aging of emission from a domestic wood stove.
Fig. S4. Time evolution of gas-phase species as measured by PTR-TOF-MS (α-pinene) and nitrate CIMS (HOM-grouped based on their number of carbons).
Fig. S5. Atomic O:C ratio as a function of carbon number for monomer and dimer products.
Fig. S6. Fraction of signal remaining (calculated as the ratio of the final signal after 12 hours to the signal at the point of the maximum mass concentration for the respective ion) for all species measured by the EESI-TOF plotted against their saturation vapor concentration (logC*).
Fig. S7. Example of time evolution for two dimer species ($C_{20}H_{32}O_9$ and $C_{19}H_{30}O_9$) measured in the particle by the EESI-TOF, illustrating calculation methods for time of maximum and decay rate.
Fig. S8. Comparison of EESI-TOF and FIGAERO-I-CIMS.
Fig. S9. Effect of OH scavenger on monomer and dimer composition.
Fig. S10. Selected time series from an experiment in which butanol was added as an OH scavenger.
Fig. S11. Comparison of EESI-TOF and SMPS measurements.
Table S1. Overview of experimental conditions.
Table S2. Decay rates and fractions remaining for selected ions as measured by the EESI-TOF.
Reference (54)

REFERENCES AND NOTES

1. K. S. Carslaw, L. A. Lee, C. L. Reddington, K. J. Pringle, A. Rap, P. M. Forster, G. W. Mann, D. V. Spracklen, M. T. Woodhouse, L. A. Regayre, J. R. Pierce, Large contribution of natural aerosols to uncertainty in indirect forcing. *Nature* **503**, 67–71 (2013).
2. F. Bianchi, T. Kurtén, M. Riva, C. Mohr, M. P. Rissanen, P. Roldin, T. Berndt, J. D. Crounse, P. O. Wennberg, T. F. Mentel, J. Wildt, H. Junninen, T. Jokinen, M. Kulmala, D. R. Worsnop, J. A. Thornton, N. Donahue, H. G. Kjaergaard, M. Ehn, Highly oxygenated organic molecules (HOM) from gas-phase autoxidation involving peroxy radicals: A key contributor to atmospheric aerosol. *Chem. Rev.* **119**, 3472–3509 (2019).
3. M. Ehn, E. Kleist, H. Junninen, T. Petäjä, G. Lönn, S. Schobesberger, M. Dal Maso, A. Trimborn, M. Kulmala, D. R. Worsnop, A. Wahner, J. Wildt, T. F. Mentel, Gas phase formation of extremely oxidized pinene reaction products in chamber and ambient air. *Atmos. Chem. Phys.* **12**, 5113–5127 (2012).
4. J. Tröstl, W. K. Chuang, H. Gordon, M. Heinritzi, C. Yan, U. Molteni, L. Ahlm, C. Frege, F. Bianchi, R. Wagner, M. Simon, K. Lehtipalo, C. Williamson, J. S. Craven, J. Duplissy, A. Adamov, J. Almeida, A.-K. Bernhammer, M. Breitenlechner, S. Brilke, A. Dias, S. Ehrhart, R. C. Flagan, A. Franchin, C. Fuchs, R. Guida, M. Gysel, A. Hansel, C. R. Hoyle, T. Jokinen, H. Junninen, J. Kangasluoma, H. Keskinen, J. Kim, M. Krapf, A. Kürten, A. Laaksonen, M. Lawler, M. Leiminger, S. Mathot, O. Möhler, T. Nieminen, A. Onnela, T. Petäjä, F. M. Piel, P. Miettinen, M. P. Rissanen, L. Rondo, N. Sarnela, S. Schobesberger, K. Sengupta, M. Sipilä, J. N. Smith, G. Steiner, A. Tomè, A. Virtanen, A. C. Wagner, E. Weingartner, D. Wimmer, P. M. Winkler, P. Ye, K. S. Carslaw, J. Curtius, J. Dommen, J. Kirkby, M. Kulmala, I. Riipinen, D. R. Worsnop, N. M. Donahue, U. Baltensperger, The role of low-volatility organic compounds in initial particle growth in the atmosphere. *Nature* **533**, 527–531 (2016).
5. A. Kürten, A. Bergen, M. Heinritzi, M. Leiminger, V. Lorenz, F. Piel, M. Simon, R. Sitals, A. C. Wagner, J. Curtius, Observation of new particle formation and measurement of sulfuric acid, ammonia, amines and highly oxidized organic molecules at a rural site in central Germany. *Atmos. Chem. Phys.* **16**, 12793–12813 (2016).
6. M. Riva, P. Rantala, J. E. Krechmer, O. Peräkylä, Y. Zhang, L. Heikkinen, O. Garmash, C. Yan, M. Kulmala, D. Worsnop, M. Ehn, Evaluating the performance of five different chemical ionization techniques for detecting gaseous oxygenated organic species. *Atmos. Meas. Tech.* **12**, 2403–2421 (2019).
7. P. J. Gallimore, M. Kalberer, Characterizing an extractive electrospray ionization (EESI) source for the online mass spectrometry analysis of organic aerosols. *Environ. Sci. Technol.* **47**, 7324–7331 (2013).
8. C. Mohr, F. D. Lopez-Hilfiker, T. Yli-Juuti, A. Heitto, A. Lutz, M. Hallquist, E. L. D'Ambro, M. P. Rissanen, L. Hao, S. Schobesberger, M. Kulmala, R. L. Mauldin III, U. Makkonen, M. Sipilä, T. Petäjä, J. A. Thornton, Ambient observations of dimers from terpene oxidation in the gas phase: Implications for new particle formation and growth. *Geophys. Res. Lett.* **44**, 2958–2966 (2017).
9. M. Brüggemann, E. Karu, T. Stelzer, T. Hoffmann, Real-time analysis of ambient organic aerosols using aerosol flowing atmospheric-pressure afterglow mass spectrometry (AeroFAPA-MS). *Environ. Sci. Technol.* **49**, 5571–5578 (2015).
10. A. Mutzel, L. Poulain, T. Berndt, Y. Iinuma, M. Rodigast, O. Böge, S. Richters, G. Spindler, M. Sipilä, T. Jokinen, M. Kulmala, H. Herrmann, Highly oxidized multifunctional organic compounds observed in tropospheric particles: A field and laboratory study. *Environ. Sci. Technol.* **49**, 7754–7761 (2015).
11. R. Zhao, C. M. Kenseth, Y. Huang, N. F. Dalleska, X. M. Kuang, J. Chen, S. E. Paulson, J. H. Seinfeld, Rapid aqueous-phase hydrolysis of ester hydroperoxides arising from Criegee intermediates and organic acids. *J. Phys. Chem. A* **122**, 5190–5201 (2018).
12. G. Isaacman-VanWertz, P. Massoli, R. O'Brien, C. Lim, J. P. Franklin, J. A. Moss, J. F. Hunter, J. B. Nowak, M. R. Canagaratna, P. K. Misztal, C. Arata, J. R. Roscioli, S. T. Herndon, T. B. Onasch, A. T. Lambe, J. T. Jayne, L. Su, D. A. Knopf, A. H. Goldstein, D. R. Worsnop, J. H. Kroll, Chemical evolution of atmospheric organic carbon over multiple generations of oxidation. *Nat. Chem.* **10**, 462–468 (2018).
13. F. D. Lopez-Hilfiker, V. Pospisilova, W. Huang, M. Kalberer, C. Mohr, G. Stefenelli, J. A. Thornton, U. Baltensperger, A. S. H. Prevot, J. G. Slowik, An extractive electrospray ionization time-of-flight mass spectrometer (EESI-TOF) for online measurement of atmospheric aerosol particles. *Atmos. Meas. Tech.* **12**, 4867–4886 (2019).
14. H. Zhang, L. D. Yee, B. H. Lee, M. P. Curtis, D. R. Worton, G. Isaacman-VanWertz, J. H. Offenberg, M. Lewandowski, T. E. Kleindienst, M. R. Beaver, A. L. Holder, W. A. Lonneman, K. S. Docherty, M. Jaoui, H. O. T. Pye, W. Hu, D. A. Day, P. Campuzano-Jost, J. L. Jimenez, H. Guo, R. J. Weber, J. de Gouw, A. R. Koss, E. S. Edgerton, W. Brune, C. Mohr, F. D. Lopez-Hilfiker, A. Lutz, N. M. Kreisberg, S. R. Spielman, S. V. Hering, K. R. Wilson, J. A. Thornton, A. H. Goldstein, Monoterpenes are the largest source of summertime organic aerosol in the southeastern United States. *Proc. Natl. Acad. Sci. U.S.A.* **115**, 2038–2043 (2018).
15. J. Liebmann, E. Karu, N. Sobanski, J. Schuladen, M. Ehn, S. Schallhart, L. Quéléver, H. Hellen, T. Hakola, T. Hoffmann, J. Williams, H. Fischer, J. Lelieveld, J. N. Crowley, Direct measurement of NO$_3$ radical reactivity in a boreal forest. *Atmos. Chem. Phys.* **18**, 3799–3815 (2018).
16. G. Eerdekens, L. Ganzeveld, J. Vilà-Guerau de Arellano, T. Klüpfel, V. Sinha, N. Yassaa, J. Williams, H. Harder, D. Kubistin, M. Martinez, J. Lelieveld, Flux estimates of isoprene, methanol and acetone from airborne PTR-MS measurements over the tropical rainforest during the GABRIEL 2005 campaign. *Atmos. Chem. Phys.* **9**, 4207–4227 (2009).
17. H. Hakola, H. Hellén, M. Hemmilä, J. Rinne, M. Kulmala, In situ measurements of volatile organic compounds in a boreal forest. *Atmos. Chem. Phys.* **12**, 11665–11678 (2012).
18. F. D. Lopez-Hilfiker, C. Mohr, M. Ehn, F. Rubach, E. Kleist, J. Wildt, T. F. Mentel, A. Lutz, M. Hallquist, D. Worsnop, J. A. Thornton, A novel method for online analysis of gas and particle composition: Description and evaluation of a filter inlet for gases and AEROsols (FIGAERO). *Atmos. Meas. Tech.* **7**, 983–1001 (2014).
19. I. Kourtchev, C. Giorio, A. Manninen, E. Wilson, B. Mahon, J. Aalto, M. Kajos, D. Venables, T. Ruuskanen, J. Levula, M. Loponen, S. Connors, N. Harris, D. Zhao, A. Kiendler-Scharr, T. Mentel, Y. Rudich, M. Hallquist, J.-F. Doussin, W. Maenhaut, J. Bäck, T. Petäjä, J. Wenger, M. Kulmala, M. Kalberer, Enhanced volatile organic compounds emissions and organic aerosol mass increase the oligomer content of atmospheric aerosols. *Sci. Rep.* **6**, 35038 (2016).
20. K. Lehtipalo, C. Yan, L. Dada, F. Bianchi, M. Xiao, R. Wagner, D. Stolzenburg, L. R. Ahonen, A. Amorim, A. Baccarini, P. S. Bauer, B. Baumgartner, A. Bergen, A.-K. Bernhammer, M. Breitenlechner, S. Brilke, A. Buchholz, S. B. Mazon, D. Chen, X. Chen, A. Dias,

J. Dommen, D. C. Draper, J. Duplissy, M. Ehn, H. Finkenzeller, L. Fischer, C. Frege, C. Fuchs, O. Garmash, H. Gordon, J. Hakala, X. He, L. Heikkinen, M. Heinritzi, J. C. Helm, V. Hofbauer, C. R. Hoyle, T. Jokinen, J. Kangasluoma, V.-M. Kerminen, C. Kim, J. Kirkby, J. Kontkanen, A. Kürten, M. J. Lawler, H. Mai, S. Mathot, R. L. Mauldin III, U. Molteni, L. Nichman, W. Nie, T. Nieminen, A. Ojdanic, A. Onnela, M. Passananti, T. Petäjä, F. Piel, V. Pospisilova, L. L. J. Quéléver, M. P. Rissanen, C. Rose, N. Sarnela, S. Schallhart, S. Schuchmann, K. Sengupta, M. Simon, M. Sipilä, C. Tauber, A. Tomé, J. Tröstl, O. Väisänen, A. L. Vogel, R. Volkamer, A. C. Wagner, M. Wang, L. Weitz, D. Wimmer, P. Ye, A. Ylisirniö, Q. Zha, K. S. Carslaw, J. Curtius, N. M. Donahue, R. C. Flagan, A. Hansel, I. Riipinen, A. Virtanen, P. M. Winkler, U. Baltensperger, M. Kulmala, D. R. Worsnop, Multicomponent new particle formation from sulfuric acid, ammonia, and biogenic vapors. *Sci. Adv.* **4**, eaau5363 (2018).

21. N. L. Ng, S. S. Brown, A. T. Archibald, E. Atlas, R. C. Cohen, J. N. Crowley, D. A. Day, N. M. Donahue, J. L. Fry, H. Fuchs, R. J. Griffin, M. I. Guzman, H. Herrmann, A. Hodzic, Y. Iinuma, J. L. Jimenez, A. Kiendler-Scharr, B. H. Lee, D. J. Luecken, J. Mao, R. McLaren, A. Mutzel, H. D. Osthoff, B. Ouyang, B. Picquet-Varrault, U. Platt, H. O. T. Pye, Y. Rudich, R. H. Schwantes, M. Shiraiwa, J. Stutz, J. A. Thornton, A. Tilgner, B. J. Williams, R. A. Zaveri, Nitrate radicals and biogenic volatile organic compounds: Oxidation, mechanisms, and organic aerosol. *Atmos. Chem. Phys.* **17**, 2103–2162 (2017).

22. B. H. Lee, F. D. Lopez-Hilfiker, E. L. D'Ambro, P. Zhou, M. Boy, T. Petäjä, L. Hao, A. Virtanen, J. A. Thornton, Semi-volatile and highly oxygenated gaseous and particulate organic compounds observed above a boreal forest canopy. *Atmos. Chem. Phys.* **18**, 11547–11562 (2018).

23. G. Stefenelli, V. Pospisilova, F. D. Lopez-Hilfiker, K. R. Daellenbach, C. Hüglin, Y. Tong, U. Baltensperger, A. S. H. Prévôt, J. G. Slowik, Organic aerosol source apportionment in zurich using an extractive electrospray ionization time-of-flight mass spectrometer (EESI-TOF-MS)— Part 1: Biogenic influences and day–night chemistry in summer. *Atmos. Chem. Phys.* **19**, 14825–14848 (2019).

24. T. Kurtén, K. Tiusanen, P. Roldin, M. Rissanen, J.-N. Luy, M. Boy, M. Ehn, N. Donahue, α-Pinene autoxidation products may not have extremely low saturation vapor pressures despite high O:C ratios. *J. Phys. Chem. A* **120**, 2569–2582 (2016).

25. K. Kristensen, Å. K. Watne, J. Hammes, A. Lutz, T. Petäjä, M. Hallquist, M. Bilde, M. Glasius, High-molecular weight dimer esters are major products in aerosols from α-Pinene ozonolysis and the boreal forest. *Environ. Sci. Technol. Lett.* **3**, 280–285 (2016).

26. P. Renard, A. E. Reed Harris, R. J. Rapf, S. Ravier, C. Demelas, B. Coulomb, E. Quivet, V. Vaida, A. Monod, Aqueous phase oligomerization of methyl vinyl ketone by atmospheric radical reactions. *J. Phys. Chem. C* **118**, 29421–29430 (2014).

27. K. C. Barsanti, J. F. Pankow, Thermodynamics of the formation of atmospheric organic particulate matter by accretion reactions—Part 1: Aldehydes and ketones. *Atmos. Environ.* **38**, 4371–4382 (2004).

28. M. Riva, L. Heikkinen, D. M. Bell, O. Peräkylä, Q. Zha, S. Schallhart, M. P. Rissanen, D. Imre, T. Petäjä, J. A. Thornton, A. Zelenyuk, M. Ehn, Chemical transformations in monoterpene-derived organic aerosol enhanced by inorganic composition. *NPJ Clim. Atmos. Sci.* **2**, 2 (2019).

29. M. J. Apsokardu, M. V. Johnston, Nanoparticle growth by particle-phase chemistry. *Atmos. Chem. Phys.* **18**, 1895–1907 (2018).

30. M. Krapf, I. El Haddad, E. A. Bruns, U. Molteni, K. R. Daellenbach, A. S. H. Prévôt, U. Baltensperger, J. Dommen, Labile peroxides in secondary organic aerosol. *Chem* **1**, 603–616 (2016).

31. T. F. Mentel, M. Springer, M. Ehn, E. Kleist, I. Pullinen, T. Kurtén, M. Rissanen, A. Wahner, J. Wildt, Formation of highly oxidized multifunctional compounds: Autoxidation of peroxy radicals formed in the ozonolysis of alkenes – deduced from structure–product relationships. *Atmos. Chem. Phys.* **15**, 6745–6765 (2015).

32. K. S. Docherty, W. Wu, Y. B. Lim, P. J. Ziemann, Contributions of organic peroxides to secondary aerosol formed from reactions of monoterpenes with O₃. *Environ. Sci. Technol.* **39**, 4049–4059 (2005).

33. P. J. Gallimore, B. M. Mahon, F. P. H. Wragg, S. J. Fuller, C. Giorio, I. Kourtchev, M. Kalberer, Multiphase composition changes and reactive oxygen species formation during limonene oxidation in the new Cambridge Atmospheric Simulation Chamber (CASC). *Atmos. Chem. Phys.* **17**, 9853–9868 (2017).

34. E. L. D'Ambro, S. Schobesberger, R. A. Zaveri, J. E. Shilling, B. H. Lee, F. D. Lopez-Hilfiker, C. Mohr, J. A. Thornton, Isothermal evaporation of α-pinene ozonolysis SOA: volatility, phase state, and oligomeric composition. *ACS Earth Space Chem.* **2**, 1058–1067 (2018).

35. L. Renbaum-Wolff, J. W. Grayson, A. P. Bateman, M. Kuwata, M. Sellier, B. J. Murray, J. E. Shilling, S. T. Martin, A. K. Bertram, Viscosity of α-pinene secondary organic material and implications for particle growth and reactivity. *Proc. Natl. Acad. Sci. U.S.A.* **110**, 8014–8019 (2013).

36. H. C. Price, J. Mattsson, Y. Zhang, A. K. Bertram, J. F. Davies, J. W. Grayson, S. T. Martin, D. O'Sullivan, J. P. Reid, A. M. J. Rickards, B. J. Murray, Water diffusion in atmospherically relevant α-pinene secondary organic material. *Chem. Sci.* **6**, 4876–4883 (2015).

37. Y. J. Li, P. Liu, Z. Gong, Y. Wang, A. P. Bateman, C. Bergoend, A. K. Bertram, S. T. Martin, Chemical reactivity and liquid/nonliquid states of secondary organic material. *Environ. Sci. Technol.* **49**, 13264–13274 (2015).

38. S. S. Steimer, A. Delvaux, S. J. Campbell, P. J. Gallimore, P. Grice, D. J. Howe, D. Pitton, M. Claeys, T. Hoffmann, M. Kalberer, Synthesis and characterisation of peroxypinic acids as proxies for highly oxygenated molecules (HOMs) in secondary organic aerosol. *Atmos. Chem. Phys.* **18**, 10973–10983 (2018).

39. R. Zhao, C. M. Kenseth, Y. Huang, N. F. Dalleska, J. H. Seinfeld, Iodometry-assisted liquid chromatography electrospray ionization mass spectrometry for analysis of organic peroxides: An application to atmospheric secondary organic aerosol. *Environ. Sci. Technol.* **52**, 2108–2117 (2018).

40. X. Zhang, R. C. McVay, D. D. Huang, N. F. Dalleska, B. Aumont, R. C. Flagan, J. H. Seinfeld, Formation and evolution of molecular products in α-pinene secondary organic aerosol. *Proc. Natl. Acad. Sci. U.S.A.* **112**, 14168–14173 (2015).

41. A. Kahnt, R. Vermeylen, Y. Iinuma, M. Safi Shalamzari, W. Maenhaut, M. Claeys, High-molecular-weight esters in α-pinene ozonolysis secondary organic aerosol: Structural characterization and mechanistic proposal for their formation from highly oxygenated molecules. *Atmos. Chem. Phys.* **18**, 8453–8467 (2018).

42. M. S. Claflin, J. E. Krechmer, W. Hu, J. L. Jimenez, P. J. Ziemann, Functional group composition of secondary organic aerosol formed from ozonolysis of α-Pinene under high VOC and autoxidation conditions. *ACS Earth Space Chem.* **2**, 1196–1210 (2018).

43. J. R. Alvarez-Idaboy, L. Reyes, N. Mora-Diez, The mechanism of the baeyer-villiger rearrangement: Quantum chemistry and TST study supported by experimental kinetic data. *Org. Biomol. Chem.* **5**, 3682–3689 (2007).

44. K. T. Malecha, Z. Cai, S. A. Nizkorodov, Photodegradation of secondary organic aerosol material quantified with a quartz crystal microbalance. *Environ. Sci. Technol. Lett.* **5**, 366–371 (2018).

45. A. Lee, A. H. Goldstein, M. D. Keywood, S. Gao, V. Varutbangkul, R. Bahreini, N. L. Ng, R. C. Flagan, J. H. Seinfeld, Gas-phase products and secondary aerosol yields from the ozonolysis of ten different terpenes. *J. Geophys. Res.* **111**, D07302 (2006).

46. R. K. Jensen, S. Korcek, M. Zinbo, M. D. Johnson, Initiation in hydrocarbon autoxidation at elevated temperatures. *Int. J. Chem. Kinet.* **22**, 1095–1107 (1990).

47. J. T. Bates, R. J. Weber, J. Abrams, V. Verma, T. Fang, M. Klein, M. J. Strickland, S. E. Sarnat, H. H. Chang, J. A. Mulholland, P. E. Tolbert, A. G. Russell, Reactive oxygen species generation linked to sources of atmospheric particulate matter and cardiorespiratory effects. *Environ. Sci. Technol.* **49**, 13605–13612 (2015).

48. K. Sindelarova, C. Granier, I. Bouarar, A. Guenther, S. Tilmes, T. Stavrakou, J.-F. Müller, U. Kuhn, P. Stefani, W. Knorr, Global data set of biogenic VOC emissions calculated by the MEGAN model over the last 30 years. *Atmos. Chem. Phys.* **14**, 9317–9341 (2014).

49. F. Paulot, D. Wunch, J. D. Crounse, G. C. Toon, D. B. Millet, P. F. DeCarlo, C. Vigouroux, N. M. Deutscher, G. González Abad, J. Notholt, T. Warneke, J. W. Hannigan, C. Warneke, J. A. de Gouw, E. J. Dunlea, M. De Mazière, D. W. T. Griffith, P. Bernath, J. L. Jimenez, P. O. Wennberg, Importance of secondary sources in the atmospheric budgets of formic and acetic acids. *Atmos. Chem. Phys.* **11**, 1989–2013 (2011).

50. D. Paulsen, J. Dommen, M. Kalberer, A. S. H. Prévôt, R. Richter, M. Sax, M. Steinbacher, E. Weingartner, U. Baltensperger, Secondary organic aerosol formation by irradiation of 1,3,5-trimethylbenzene–NOₓ–H₂O in a new reaction chamber for atmospheric chemistry and physics. *Environ. Sci. Technol.* **39**, 2668–2678 (2005).

51. S. Schobesberger, F. D. Lopez-Hilfiker, D. Taipale, D. B. Millet, E. L. D'Ambro, P. Rantala, I. Mammarella, P. Zhou, G. M. Wolfe, B. H. Lee, M. Boy, J. A. Thornton, High upward fluxes of formic acid from a boreal forest canopy. *Geophys. Res. Lett.* **43**, 9342–9351 (2016).

52. A. Jordan, S. Haidacher, G. Hanel, E. Hartungen, L. Märk, H. Seehauser, R. Schottkowsky, P. Sulzer, T. D. Märk, A high resolution and high sensitivity proton-transfer-reaction time-of-flight mass spectrometer (PTR-TOF-MS). *Int. J. Mass Spectrom.* **286**, 122–128 (2009).

53. M. Kulmala, J. Kontkanen, H. Junninen, K. Lehtipalo, H. E. Manninen, T. Nieminen, T. Petäjä, M. Sipilä, S. Schobesberger, P. Rantala, A. Franchin, T. Jokinen, E. Järvinen, M. Äijälä, J. Kangasluoma, J. Hakala, P. P. Aalto, P. Paasonen, J. Mikkilä, J. Vanhanen, J. Aalto, H. Hakola, U. Makkonen, T. Ruuskanen, R. L. Mauldin III, J. Duplissy, H. Vehkamäki, J. Bäck, A. Kortelainen, I. Riipinen, T. Kurtén, M. V. Johnston, J. N. Smith, M. Ehn, T. F. Mentel, K. E. J. Lehtinen, A. Laaksonen, V.-M. Kerminen, D. R. Worsnop, Direct observations of atmospheric aerosol nucleation. *Science* **339**, 943–946 (2013).

54. N. M. Donahue, W. Chuang, M. Schervish, Gas-phase organic oxidation chemistry and atmospheric particles, in *Advances in Atmospheric Chemistry. Volume 2: Organic Oxidation and Multiphase Chemistry* (World Scientific, 2019), pp. 199–317.

Citation: V. Pospisilova, F. D. Lopez-Hilfiker, D. M. Bell, I. El Haddad, C. Mohr, W. Huang, L. Heikkinen, M. Xiao, J. Dommen, A. S. H. Prevot, U. Baltensperger, J. G. Slowik, On the fate of oxygenated organic molecules in atmospheric aerosol particles. *Sci. Adv.* **6**, eaax8922 (2020).

Science Advances

On the fate of oxygenated organic molecules in atmospheric aerosol particles

V. Pospisilova, F. D. Lopez-Hilfiker, D. M. Bell, I. El Haddad, C. Mohr, W. Huang, L. Heikkinen, M. Xiao, J. Dommen, A. S. H. Prevot, U. Baltensperger and J. G. Slowik

ARTICLE TOOLS	http://advances.sciencemag.org/content/6/11/eaax8922
SUPPLEMENTARY MATERIALS	http://advances.sciencemag.org/content/suppl/2020/03/09/6.11.eaax8922.DC1
REFERENCES	This article cites 53 articles, 5 of which you can access for free http://advances.sciencemag.org/content/6/11/eaax8922#BIBL
PERMISSIONS	http://www.sciencemag.org/help/reprints-and-permissions

Use of this article is subject to the Terms of Service